PLOS COMPUTATIONAL BIOLOGY

RESEARCH ARTICLE

With an eye on uncertainty: Modelling pupillary responses to environmental volatility

Peter Vincent[☯]*, **Thomas Parr**[☯], **David Benrimoh**[☯], **Karl J Friston**[☯]

Wellcome Trust Centre for Neuroimaging, Institute of Neurology, University College London, London, United Kingdom

☯ These authors contributed equally to this work.
* peter.vincent.14@ucl.ac.uk

OPEN ACCESS

Citation: Vincent P, Parr T, Benrimoh D, Friston KJ (2019) With an eye on uncertainty: Modelling pupillary responses to environmental volatility. PLoS Comput Biol 15(7): e1007126. https://doi.org/10.1371/journal.pcbi.1007126

Editor: Adrian M Haith, Johns Hopkins University, UNITED STATES

Received: October 7, 2018

Accepted: May 23, 2019

Published: July 5, 2019

Data Availability Statement: The spm_MDP_VB_X.m Matlab script, used in this work, is available as part of the SPM12 package, downloadable at http://www.fil.ion.ucl.ac.uk/spm/.

Funding: The authors received no specific funding for this work.

Competing interests: The authors have declared that no competing interests exist.

Abstract

Living creatures must accurately infer the nature of their environments. They do this despite being confronted by stochastic and context sensitive contingencies—and so must constantly update their beliefs regarding their uncertainty about what might come next. In this work, we examine how we deal with uncertainty that evolves over time. This prospective uncertainty (or imprecision) is referred to as volatility and has previously been linked to noradrenergic signals that originate in the locus coeruleus. Using pupillary dilatation as a measure of central noradrenergic signalling, we tested the hypothesis that changes in pupil diameter reflect inferences humans make about environmental volatility. To do so, we collected pupillometry data from participants presented with a stream of numbers. We generated these numbers from a process with varying degrees of volatility. By measuring pupillary dilatation in response to these stimuli—and simulating the inferences made by an ideal Bayesian observer of the same stimuli—we demonstrate that humans update their beliefs about environmental contingencies in a Bayes optimal way. We show this by comparing general linear (convolution) models that formalised competing hypotheses about the causes of pupillary changes. We found greater evidence for models that included Bayes optimal estimates of volatility than those without. We additionally explore the interaction between different causes of pupil dilation and suggest a quantitative approach to characterising a person's prior beliefs about volatility.

Author summary

Humans are constantly confronted with surprising events. To navigate such a world, we must understand the chances of an unexpected event occurring at any given point in time. We do this by creating a model of the world around us, in which we allow for these unexpected events to occur by holding beliefs about how volatile our environment is. In this work we explore the way in which we update our beliefs, demonstrating that this updating relies on the number of unexpected events in relation to the expected number. We do this by examining the pupil diameter, since—in controlled environments—changes in pupil

diameter reflect our response to unexpected observations. Finally, we show that our methodology is appropriate for assessing the individual participant's prior expectations about the amount of uncertainty in their environment.

Introduction

The role of the noradrenergic (NA) system in decision making [1] and encoding uncertainty [2] has been explored in great depth, with many studies using pupillary dilation as an index of changes in central adrenergic signalling [3–6]. A central theme of this work is the role of NA in contextualising perceptual inference and planning. This has an interesting connection to the P3 evoked response potential seen in EEG paradigms [7]. The amplitude of the P3b wave increases following presentation of surprising stimuli [8,9] and is thought to signal a change in beliefs about the underlying environmental contingencies [9]–i.e., the updating of context [10]–and might be mediated by NA [1]. However, these accounts of the role of NA in signalling surprise often focus on transient responses following a single unexpected event. Here, we extend this work to show that pupil dilatation tracks a subject's long-term beliefs (that is, tonic changes to the baseline pupil diameter), spanning multiple aberrant events and how these allow the participant to infer the precision of their environmental dynamics. Precision here refers to the predictability of the next state of the world, given the current state.

Formally, we appeal to the notion of a generative model. This is central to theoretical treatments of the Bayesian brain and, more generally, active inference. These accounts frame brain function as a process of inference that depends upon an internal generative (predictive) model comprising prior beliefs about variables in the world, and (likelihood) beliefs about how these give rise to sensory data. On observing sensory data, creatures can use their internal model to update posterior beliefs about their environments. Posterior beliefs can then be used to compute empirical prior beliefs about the future (i.e., planning as inference), using temporal contingencies in the generative model. Our focus here is how the brain handles uncertainty about these contingencies.

The encoding of uncertainty is essential in enabling animals to predict confidently (or not) what might happen next [11]. From the perspective of the Bayesian brain, this is the process of using beliefs about the past to form (empirical) prior beliefs about the present. Crucially, the confidence (precision) in these priors determines the relative weighting of prior and sensory influences on perceptual or state inference. This has relevance for the role of abnormal prior beliefs in pathology, where under-confident priors fail to contextualise inferences drawn from sensory data or where excessively confident priors support false inferences in the presence of contradictory sensory data [12]. Of particular relevance to this work are those conditions that have been associated with abnormal NA signalling—for example, autism [13,14].

We start by introducing a few technical concepts. Following this, we describe our experimental design and data collection. With these data, we test the hypothesis that the pupil diameter closely tracks the precision inferred by the participant in a volatile setting. We build on this formulation to propose a technique that quantifies prior beliefs, which could be used in a clinical context to phenotype individuals, in terms of their prior beliefs about precision and volatility (e.g., that might underwrite autistic symptoms).

Precision, inference and Markov decision processes

Adaptive engagement with the world requires an understanding of our sensations in terms of the latent (hidden or unobservable) states that generated them. This requires an internal

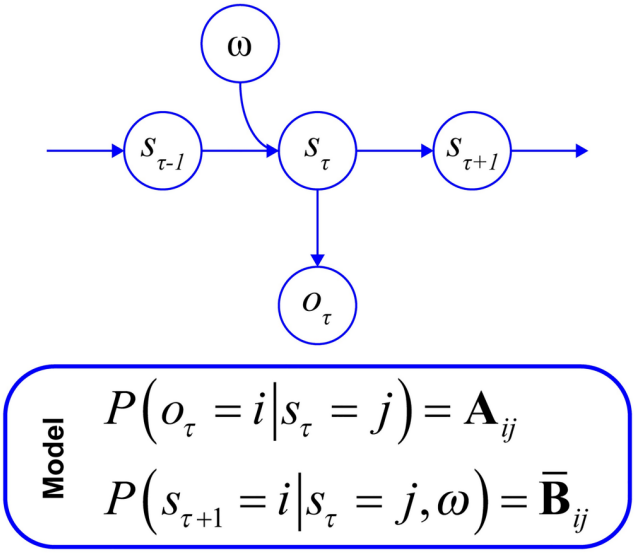

Fig 1. A (simplified) Bayes net. This is a form of graphical notation that expresses the conditional dependencies in the generative model. Random variables are shown in circles, with arrows indicating causal influences. The progression from one state (s_τ) to the next ($s_{\tau+1}$) is affected by the precision (ω) of the transition matrix. This stochasticity results in randomness in the observed outcomes (o_τ). The panel below specifies the parameterisation of this model. Notably, in addition to (likelihood) beliefs about how states generate data (**A**), and beliefs about state transitions (**B**), we need prior beliefs about the precision of these transitions. These take the form of a gamma distribution, $P(\omega) \propto \beta e^{-\beta \cdot \omega}$, where the current prior belief (ω) is a function of the most recent posterior beliefs ($\boldsymbol{\beta}$). This has the convenient property that the expectation of the prior beliefs as we update them are the value of the most recent posterior beliefs [22].

https://doi.org/10.1371/journal.pcbi.1007126.g001

(generative) model of the world that can be used to make predictions about sensory input [15]. These generative models are necessarily complicated (i.e., usually deep, dynamical and nonlinear), to capture the subtleties of our (deep, dynamical and nonlinear) environment. Despite the complexity of such models, they can be constructed by combining relatively simple models [16]. The simplest that accounts for perceptual inference and planning—in a changing environment—is a Markov decision process (MDP) [17]. Technically, in this paper we use a hidden Markov model (as we do not model any decisions), but we retain the MDP rhetoric to emphasise that these results generalise to situations that require active sensing of the world [17,18]. In the following section we provide a brief outline of the inversion of this type of generative model. Readers familiar with this sort of modelling are invited to skip this section.

An MDP treats the world as comprising a series of states (s) that are hidden from an observer. The transitions among these states over time represent the (stochastic) dynamics of the environment, and are defined by a (square) transition matrix that we denote by **B** (see Fig 1 for a Bayes net representation of this process). These states give rise to observable outcomes that act as the observer's sensory stimuli. The relationship between the hidden states and the outcomes they generate is expressed as a likelihood matrix, **A**. These probability distributions are not trivial: to motivate their importance we appeal to the Good Regulator Theorem [19]. This theorem says that 'every good regulator of a system must be a model of that system.' From this, one may intuit that if a creature inhabits, and wishes to interact with, an environment defined by stochastic state transitions, this creature must be able to estimate the precision (i.e., the negative entropy) of these transition densities. The ensuing inference about environmental dynamics is intertwined with beliefs regarding the likelihood mapping from states to outcomes, since it is only these outcomes that an agent can observe [17]. If the dynamics of the environment are deterministic, and state-to-outcome mappings are well understood, the agent

is likely to have precise beliefs about the nature of its environment, and is therefore able to accurately predict what it may expect to see in the future [20]. However, when these mappings from states to outcomes are not deterministic and where state transitions are themselves stochastic—the agent is presented with a confound, since poor inferences about the nature of state-to-outcome mappings may have a detrimental effect on inferences about state transitions [20,21].

We represent these imprecise state-to-outcome mappings and state-to-state transitions in the **A** and **B** matrices, respectively (Fig 2). Imprecise state transitions (a non-deterministic **B** matrix) define a volatile environment. In other words, volatility is equivalent to the inverse precision of the **B** matrix. In a volatile world, even if an animal accurately infers the likelihood mappings and state transitions, the stochastic nature of these dynamics means the agent's beliefs about what will happen next are necessarily imprecise [22]. Imprecise beliefs over state transitions leave the animal with no way of predicting what might come next. This has been referred to as 'unexpected uncertainty', in contrast to 'expected uncertainty' (that maps to imprecision of **A**) [2,6].

Volatility and pupil dilation

Previous work has suggested that acetylcholine (ACh) and noradrenaline (NA) act as the neurochemical analogues of the precision over state-outcome mappings (i.e. the **A** matrix) and the precision over state transitions (defining the empirical prior and **B** matrix) [2] respectively. In other words, ACh is thought to be involved in signalling confidence in our beliefs about the likelihood of what we might see, in a given state, while NA moderates our confidence in prior beliefs about the state we may find ourselves in next [2,3,5,23,24]. In this work, we use these proposed relationships—between central noradrenergic signalling and volatility signalling—to motivate predictions about changes in pupil diameter based on environmental volatility. Given that circuits in the brain—that update beliefs over the likelihood mappings from states

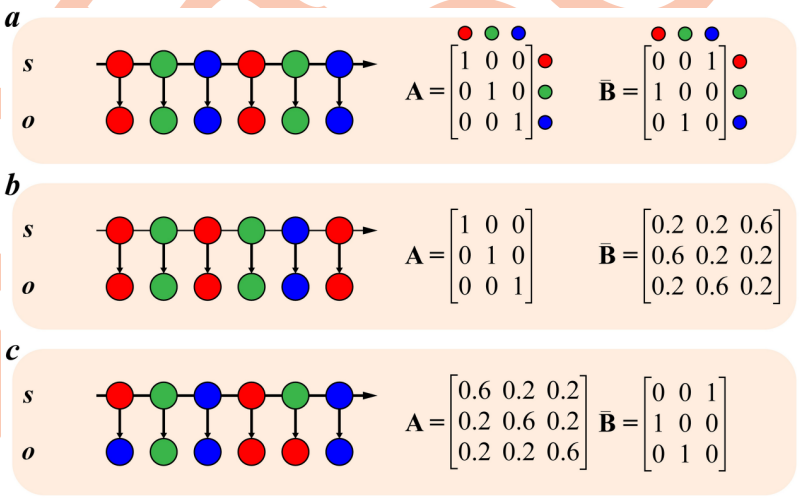

Fig 2. Sequences of outcomes emerging from random transition dynamics. Fig 2a shows the sequence of outcomes (*o*) produced by the sequence of states (*s*) when the transition matrices for both sequences are deterministic. Fig 2b shows the sequence of states, and outcomes those states generate, when the matrix defining the transitions between states (**B**) is not deterministic. Even though the transitions from states to outcomes are still deterministic, as in Fig 2a, the final sequence of outcomes is different. In Fig 2c we show the consequences of introducing randomness into the transitions (matrix **A**) from states to events. The sequence of states remains the same as in Fig 2a, but the outcomes generated by each state are random, resulting in a different sequence of outcomes. Figs 2a and 2c demonstrate how randomness in the transition matrices can results in unpredictable sequences of outcomes.

https://doi.org/10.1371/journal.pcbi.1007126.g002

to outcomes—are thought to use ACh as a transmitter [2,23,25–29], a potential confound arises: pupil diameter, particularly the tonic changes examined in this work, may also depend on beliefs about the likelihood of certain stimuli. We therefore consider the possibility that beliefs about sensory mappings may confound the effects of beliefs about state transitions on the pupillary response; acknowledging that beliefs about the likelihood might also vicariously influence beliefs about transitions. Put simply, an unexpected observation could plausibly be explained by imprecision in either the **A** or the **B**-matrix.

Parameterising volatility

To optimise beliefs about environmental uncertainty (i.e., precisions), we must first specify how precisions are parameterised. To pursue this formally, we express the precisions as inverse temperature parameters, such that the precision of state transitions is given by ω. This adjusts a (source) transition **B** matrix by virtue of a Gibbs measure (i.e., a softmax function), as shown in Eq 1. Here, precision is an exponent on the elements of the transition matrix, which is then normalised, to produce the agent's beliefs about state transitions [22].

$$\bar{\mathbf{B}}_{\tau,ij} = \mathbf{B}_{ij}^{\omega} \Big/ \sum_k \mathbf{B}_{ik}^{\omega} \tag{1}$$

Eq 1 describes how transition matrices are generated from a source matrix. This produces the transition matrices shown in Fig 3, with all 4 derived from the same 'source' matrix. Intuitively, a high prior precision reflects high confidence in prior beliefs, and would be represented by a large value of ω. If ω were to equal infinity, this would represent absolute confidence, and results in a purely deterministic transition matrix, as is shown in Fig 3a. Smaller values of ω (Fig 3b–3d) represent increasingly less precise beliefs, resulting in increasingly stochastic transition matrices, and a greater propensity to accommodate randomness in the environment.

The updated, normalised (denoted by the bar notation), **B** matrix is then used to update the expected precision given new sensory outcomes. Under ideal Bayesian observer assumptions [22] this update can be cast as a gradient ascent on variational free energy (a lower bound on log model evidence). Specifically, this scheme updates the volatility (inverse precision, $\beta = \omega^{-1}$) using the sum of prediction errors, weighted over all possible transitions, as shown in Eq 2. These prediction errors represent the difference between the observed state transition and the expected state transition, where the expected transition is calculated using the updated **B** matrix calculated in Eq 1. The ensuing error term is shown in Eq 3.

$$\dot{\boldsymbol{\beta}} = \beta - \sum_{\tau} \ln(\mathbf{B}_{\tau}) \cdot \boldsymbol{\varepsilon}_{\tau} - \boldsymbol{\beta} \tag{2}$$

$$\boldsymbol{\varepsilon}_{i,\tau} = (s_{\tau+1} - \bar{\mathbf{B}}_{\tau,i}) \cdot s_{\tau} \tag{3}$$

$$s_{\tau} = \boldsymbol{\sigma}(\mathbf{v}_{\tau});\ \mathbf{v}_{\tau} = \omega \cdot \ln(\mathbf{B}_{\tau} \cdot s_{\tau+1}) + \ln(\mathbf{A} \cdot o_{\tau}) - \ln(s_{\tau}) \tag{4}$$

Eqs 2 and 3 show how the inferred volatility is inextricably linked to violations of expected transitions, as inferred by the subject [22]. Here, σ refers to the softmax function. Importantly, the non-italic β in Eq 2 represents the prior beliefs an agent has regarding the volatility of the environment (so $\beta^{-1} = \omega$ are the prior beliefs over precision). Eq 2 therefore shows how the agent's posterior beliefs about the current environmental volatility (β) depends on their prior beliefs. The formulation in Eq 3 provides a useful intuition on belief updating for volatility or precision. It says that, for every possible current state, we compute the difference between the expected next state and the posterior beliefs about that state. These errors are weighted by the posterior probability of the current state. Larger errors then induce greater updates in beliefs

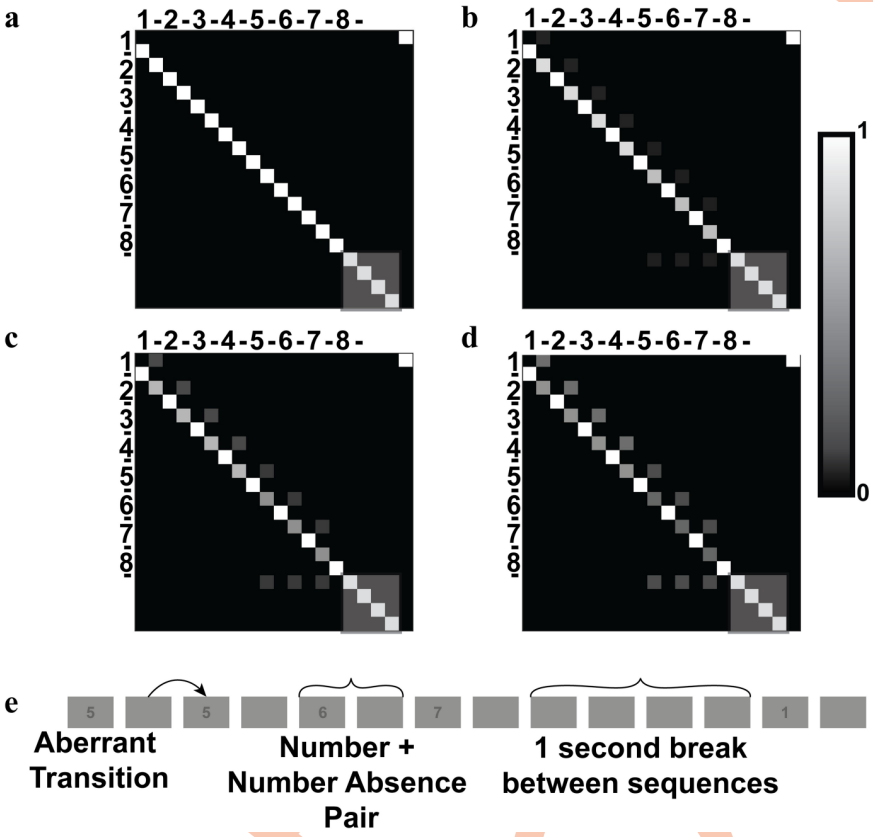

Fig 3. B matrices created for the generative process. Lighter values indicate probabilities closer to 1. As the precision decreases, shown in Figs 3a through 3d, the probability of a number-absence state transitioning to the next number decreases, while the probability of a transition to the preceding number increases. The grey transparent box covers transitions into and within the final 1s break. Separate states are required for each of the number-absence states to ensure this matrix generates a reliable sequence of numbers. Number-absence states following 5,6,7 may transition to the first of the block of 4 number-absence states as the precision decreases, to ensure that the sequence of numbers is always 8 long. These matrices can result in unexpected sequences, as shown in Fig 3e, which is drawn from the matrix defining a scenario with precision = 0.39, since it only has one error.

https://doi.org/10.1371/journal.pcbi.1007126.g003

about the volatility. Framing belief updating in terms of state prediction errors connects this aspect of active inference to recent work suggesting that much of noradrenergic phenomenology can be reproduced by appealing to similar error terms [30].

Eq 4 shows how we estimate posterior beliefs about the states, and the influence of the volatility on this belief updating [22]. This shows that, in a highly volatile world (low ω), the influence of beliefs about the future and past should have little influence over beliefs about the present, and we should rely to a greater extent upon sensory evidence. In contrast, in minimally volatile environments, we should depend more upon empirical priors from the past and future. When inferring state trajectories, we can use these posterior beliefs to evaluate Eq 3 and update beliefs about volatility.

There is a large literature on modelling of volatility in dynamical systems that rely upon autoregressive or Kalman filter like models. While important for cognitive sciences and psychology [31,32], these also find application in the domain of financial modelling and economics [33,34]. Some of these approaches rely upon the use of stochastic differential equations for continuous variables (or their associated density dynamics [35]), while others rely upon probability transition matrices. In the former, volatility is simply the variance of random

fluctuations, while in the latter it takes the form of a temperature parameter. Common to all, is the notion that the current value of a latent variable does not deterministically predict the next value. All explicitly or implicitly appeal to the imprecision of predictions about the next state, given the current state, as a measure of volatility.

Previous work has considered the updating of precisions in continuous state space models, using a hierarchical gaussian filter [36]. In this scheme, beliefs are held at multiple hierarchical levels, with belief updating driven by prediction errors. The precisions at each level are dynamic, and encode the uncertainty (or the volatility) about fluctuating continuous states of the environment [36]. Other approaches have considered a delta-rule style belief updating, which has been combined with Bayesian approaches to form a Bayesian delta rule [37,38]. These formulations have previously been used to examine the relationship between noradrenergic signalling and the estimation of volatility in both a neurotypical setting, with and without reward, [6,38] and in the case of patients with autism [14]. Indeed, optimising beliefs about the uncertainty of state transitions is an essential feature of cognitive flexibility, allowing us to anticipate changes in task contingencies. This means we can assess the relevance of recent events in predicting what might come next. This regulation of beliefs is synonymous with the learning rate in reinforcement learning [6,24,38,39].

In this work we focus on the uncertainty about the environmental contingencies. By formalising the Bayesian updating thought to occur in the brain [6,22,40], we can quantify the prior precision (i.e., confidence) participants afford their beliefs about environmental volatility by examining the effect on the belief-updating when presented with a unpredictable outcomes [22]. Crucially, our model makes predictions about the online encoding of uncertainty and accompanying pupillometric responses. This allows us to examine the tonic responses of the pupil without using summary statistics, as in previous work [6,41]: usually, trial-to-trial fluctuations in the pupil diameter are measured by taking the average dilation or the change relative to baseline. In this work, we generalise this examination of the trial-to-trial fluctuations in pupil diameter by explicitly parametrising it as a function of inferred precision [22]. This allows us to quantify a participant's prior precisions over environmental volatility based upon observable (pupillometry) responses—a capability that holds promise for applications in theoretical, computational and clinical neuroscience [14,22,42].

Materials and methods

To test the hypothesis that pupillary responses are, in part, mediated by the encoding of uncertainty, we assessed the evidence for alternative models of pupillary dilatation afforded by pupillometry data from 9 healthy participants. We generated plausible models to account for pupillary responses, considering optical factors, our formulation of the inferred environmental volatility, and possible interactions between these factors (i.e. how beliefs about environmental volatility moderate the pupillary response to luminescence). In this section, we explain the design and rationale of the stimuli, the pupillometry data collection protocol, stimulus generation and model specification.

Ethics statement

The study was approved by the UCL Research Ethics Committee (Project ID Number 4356/002). Both oral and written informed consent was obtained from all participants.

Pupillometry data collection

We recruited 9 participants between the ages of 18–35 with no reported psychiatric history and neurotypical development. All participants' data are included in the analysis, and all

participants completed the 16 blocks. Each block lasted for just over 2 minutes; allowing for short breaks between blocks (to avoid discomfort). Each session lasted for around 1 hour. Participants rested their head in a chinrest 0.5m away from a stimulus presentation screen. Dark numbers on a grey background were used to reduce the effect of pupillary dilatation in response to changes in illumination [37], and the lights were dimmed (high illumination leads to a constricted pupil and restricted dilatation). Quiet was maintained during each experiment to avoid dilation in response to auditory cues [43], which would effect the level of surprise [6]. Pupil area was monitored in the left eye using an EyeLink 1000 desktop mount (SR Research, sampling rate: 1000Hz), with calibration performed before the first experiment, as well as after any periods where the participant moved from the chin rest.

While fluctuations in pupil diameter can be attributed to a luminance effect, due to the presentation of numbers on the screen, we note that this pupil dilation could alternatively (and perhaps also) be due to increased attention [44]. This effect has been reported during auditory paradigms: a recent study showed that the conscious processing of regularities in an auditory paradigm induces a pupillary dilation [4,45,46].

Task procedure and stimulus generation

To measure the pupillary response to changes in environmental volatility, we presented sequences of numbers increasing from 1 to 8. These were generated using a probability transition matrix (details below), analogous to that used in the generative model (see Fig 2). We chose numbers because prior exposure to number sequences means that participants are 'over-trained', and do not need to learn new sequences. To increase the volatility of this stimulus, we decreased the precision of the transition matrix used to generate the sequence. This introduced violations of the 1–8 sequence. Every sequence, irrespective of the number of violations, comprised 8 numbers. Each number was presented for 250ms, followed by a 250ms with no stimulus. In other words, each number was always followed by the absence of a number, such that each of these pairs lasted for 500ms. After 8 pairs, there was a delay for 1 second. The small 250ms spaces between numbers were required to make transitions distinct (for example, without these interludes a transition from a 2 back to a 2 would simply look like an extended presentation of the number 2). The 1 second breaks between sequences helped prevent transitions such as 8 to 1 as one sequence ends and another began immediately after—as this could equally well be seen as a an unexpected transition. Numbers were presented in a dark font on a grey screen; a truncated example of a sequence is shown in Fig 4e.

To account for the 250ms number absences between the numbers, and a final 1s break between states (comprising 4 consecutive 250ms number absences), we required a 20x20 probability transition matrix. We ensured that all numbers invariably transitioned to a number absence state, but number absence states could stochastically transition back to the previous number, or to the next number. Specifically, we specified the probability of the 'correct' transition (i.e. to the next number numerically) as 0.99, and then split the remaining probability mass among the remaining possible state transitions. We then selected 4 levels of volatility that would give, on average, 0, 1, 2 or 3 aberrant transitions within a sequence of 8 numbers. These volatilities were used to create the matrices shown in Fig 3a–3d. To generate the sequences shown in Fig 4, we iterated using the respective matrix 20 times, and—if the resultant sequence was suitable (i.e. composed of 8 numbers, to ensure all sequences are the same length)–the sequence was accepted; otherwise we generated a new sequence.

A single block comprised 25 sequences in total and each participant performed 16 blocks. The first of these sequences was simply 1–8. The remaining 24 sequences were divided into 8 sets of 3 sequences. Each set was assigned a level of precision, and the appropriate **B** matrix

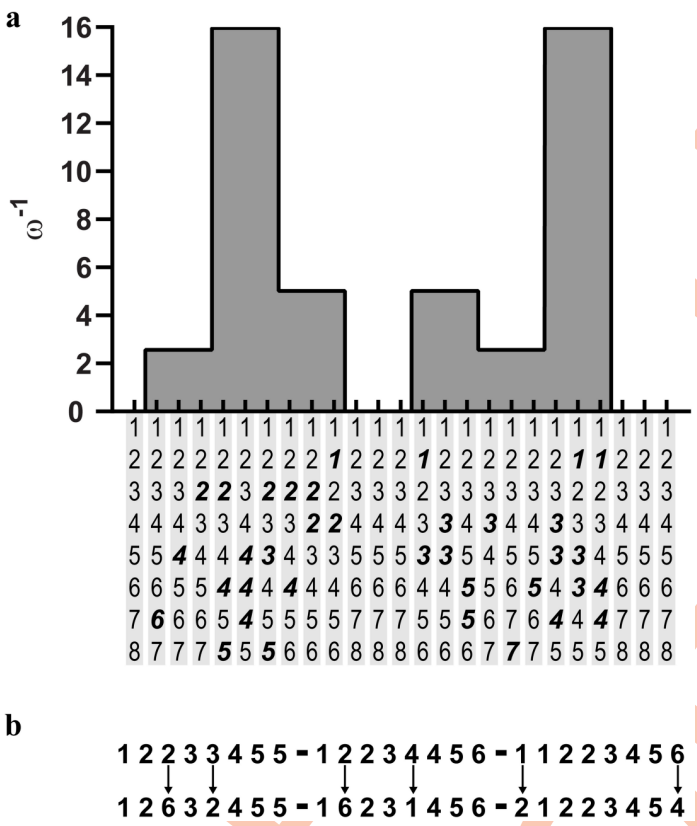

Fig 4. Sequences and their volatility. 25 sequences are presented in each block. The first sequence is 1–8. The following 24 sequences are placed into 8 sets; each set has a predetermined volatility; alternatively, the y-axis gives the volatility of the generative process. The exact sequences are shown hanging below the x-axis in Fig 4a, where unexpected numbers resulting from an aberrant transition are highlighted in bold font. ω^{-1} is used here to distinguish the volatility of the generative process from the participants' inferred volatility β. Fig 4b shows the composition of combination sequences. The same set of 25 sequences is taken, in the same order, to generate the combination sequences. Two numbers in each sequence are exchanged for different numbers to generate a new sequence. The upper row shows sequences with varying degrees of volatility (but precise likelihood probabilities), while the lower row shows these same sequences augmented as if they were generated from imprecise likelihood distributions.

https://doi.org/10.1371/journal.pcbi.1007126.g004

was used to generate each of the 3 sequences. The precisions of the sequences throughout the experiment, and the sequences themselves, are shown in Fig 4. These sequences and their ordering were kept constant throughout all 16 blocks. To ensure participants maintained focus, we asked them to perform an incidental task: they were asked to tap on a tap-counter every time they saw a specific number (this number was different in each block). They were explicitly asked not to count how many times they saw the target number, but rather to focus on the next number (which they were told should always be 1 greater than the number they just saw).

Above, we noted the possibility of an interaction between beliefs about likelihood mappings and state transitions. In the context of these sequences, we looked for this interaction by creating combination sequences for 8 of the 16 blocks that participants completed. In these sequences, we took the basic sequences given in Fig 4, randomly selected 2 numbers and switched them for different numbers. Examples of these switches and the resultant sequences are given in Fig 4.

In summary, each participant completed 16 blocks. 8 are composed of the basic sequences detailed in Fig 4, while 8 are combination sequences, constructed in the manner shown in

Fig 4. Importantly, in each set of 8 blocks, the sequence of numbers was exactly the same. In a post-hoc debrief, participants were asked what they noticed about the sequences. None reported that the sequences were the same (either within the sets of 8 blocks or between the sets of 8 blocks), and all commented that they simply ignored the random numbers in the combination sequences, which has a heuristic similarity to the results shown by Parr and Friston (random stimuli that have no informative value are down sampled/ignored) [47]. Following pre-processing (detailed in the next section), we compared the time series generated from the basic sequences to those generated by the combination sequences. We selected random sections of the time series and used their mean and variance to look for a statistically significant difference in the time series and found none. We ran all analyses (see sections below) on both data sets separately, yielding similar results (though with somewhat larger error due to increased noise from reducing the sample size—see 9a insert for an example of these results). We were therefore able to pool the blocks, and do not make any further distinction between the basic and combination sequences.

Pupillometry data analysis

Following acquisition, all data were processed with the same protocols, which are well established in the literature. First, blinks were removed by identifying data for which the pupil diameter is 0. These time points are padded by 150ms either side, removed, then replaced by linear interpolation [6,48]. We then regressed out the effect of a temporal drift, the presence of a violation (of both types in the combination series) and the presence of a target number (those requested for the counting task) [6,49]. The data were then mean centered, low-pass filtered below 10Hz, and down-sampled to 10Hz. Since the analysis we performed later was in the time domain, we had no need to respect the Nyquist frequency. Down sampling to 10Hz from 1000Hz was required since the predictions we generated (see next section) were generated at 4Hz.

Finally, the data were normalised by their standard deviation, such that the final time series represents the number of standard deviations from the mean diameter. This ensured that we could average the data over subjects, while allowing for the fact that some participants' responses may have overall smaller pupillary responses due to differential sensitivity to the luminance of the screen. At this point, the data from all 16 blocks for a given participant were averaged together; such that our data-space now comprises 9 time-series (one for each participant) performing exactly the same tasks. This allowed us to construct an 'event related average', analogous to the approach used to find evoked responses in EEG research [50]. The grand mean of this average, over subjects, is shown in Fig 5.

Simulations

To test our hypothesis (that the central adrenergic system mediates Bayes optimal updating of beliefs over volatility), we simulated belief updating in response to our stimuli. The simulations were performed by iterating Eqs 1, 2, 3 and 4 in a Matlab script customised from spm_MDP_VB_X.m (details in supporting materials). This scheme inverts a generative model based on an MDP to provide free energy minimizing solutions to the underlying active inference problem (that entails the solution to Eq 2). Inference about precision is assumed to proceed over a longer time-scale than state inference (inference about the precision requires beliefs about the current state, which must be inferred from the observed outcomes over a number of time-steps). From Eq 2 it is clear that the inferred volatility is dependent on the prior beliefs over precision (β^{-1}). We therefore generated simulations of ω with a range of β^{-1} from 0.3–20. The inverse of the ensuing precision is then taken to be the inferred volatility.

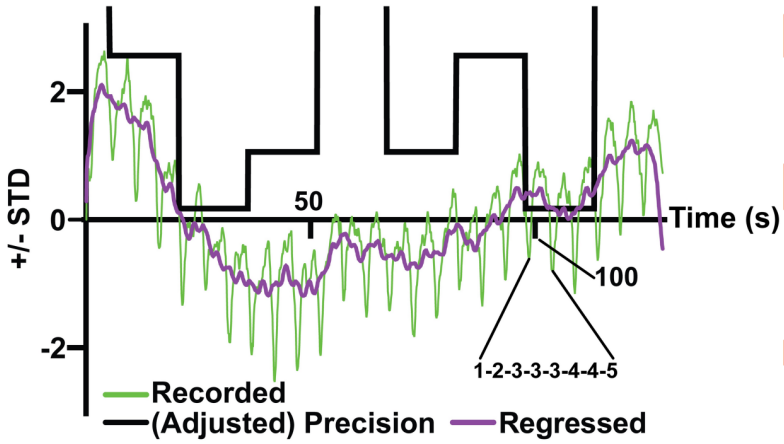

Fig 5. Grand mean of data. This figure shows the data when averaged across all blocks and participants. There are 25 oscillations, which correspond to the 25 sequences, and we explain this in terms of an optical effect. In the next section, we propose that the slow fluctuations that characterise this data are explained best by inferred precision. The grand mean data is shown in green, while the data with the fluctuations regressed out is shown in purple. A trace indicating the precision of the sequences is overlaid—referred to as the adjusted precision, to differentiate from the inferred precision of the participants.

https://doi.org/10.1371/journal.pcbi.1007126.g005

Different prior precisions have a profound effect on the shape and scale of belief updating, as can be seen in Fig 6. These simulations are generated at a 4Hz frequency (notice this is the frequency of the stimulus), and we therefore need to up-sample this to 10Hz (by linear interpolation) for comparison with our empirical data. While it may appear as if the time-course in Figs 5 and 6 depends only upon whether numerical sequences are violated, it is actually a little subtler than this. The nature of the response is highly dependent on the prior precision of the participant and the participant's current inferences about precision. Furthermore, in the short periods of differing volatility that our experiment affords, participants with particularly high beliefs over the environmental volatility are less likely to track these small changes, since they are already expected, whereas participants with strong beliefs over the precision of the environment experience a greater prediction error and will track these changes. Notably, even as the

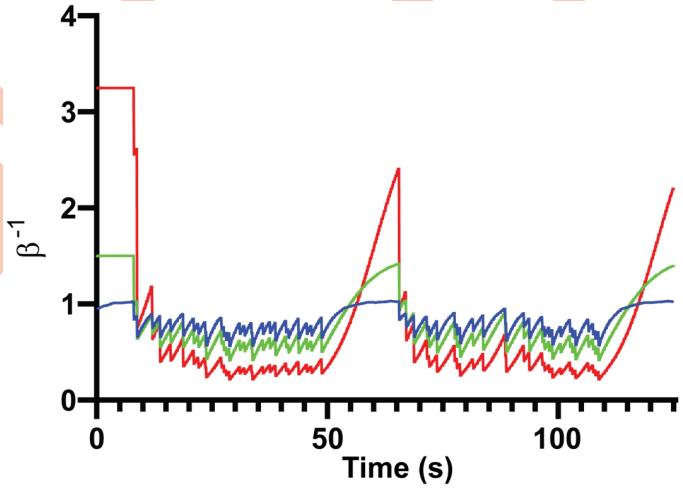

Fig 6. Simulations of the inferred precision. Three simulations are generated with prior precisions of 1, 1.5 and 3.25, in blue, green and red respectively (see Eq 2 for a formal definition of prior precision).

https://doi.org/10.1371/journal.pcbi.1007126.g006

pupil responds to individual aberrations that allow updating of beliefs about precision, the tonic state will change to reflect these beliefs.

Model space

To test for the hypothesized effects of the inferred precision on pupil diameter, we took the grand mean of the data to generate a pupillometry time series, averaged over all blocks for all participants. Noting the shape of the data (Fig 5), we wanted to consider the balance between optical effects (changes in luminance due to the numbers presenting on the screen) and the updating of inferred environmental precision. With this in mind, we generated 4 plausible models, summarised in Table 1. The explanatory variables detailed in this table accommodate the photic stimulation (effect of numbers on the screen) in each model, and then build on this to consider more comprehensive models of pupillary responses. Model 1 comprises photic stimulation only. This represents a null model. Model 2 contains the photic stimulation and an interaction effect, where the inferred precision acts in concert (i.e. non-additively) with the optical effects. Model 3 contains the photic stimulation and the inferred precision, suggesting that the inferred precision acts independently from optical effects to drive pupillary dilation. Finally, model 4 contains all three effects (optical, interaction and precision). These models are summarised in Table 1. We included a further two interesting models: Model 5 supposes that there are no tonic effects beyond a slow return to baseline following an unexpected event (note this supposes that the tonic effects are simply a due to slow dynamics of the pupil in response the phasic effects). Model 6 supposes that the participant immediately knows the current environmental volatility, rather than having to infer it from the observed data.

Model fitting

Taking inspiration from the field of neuroimaging, we analysed the pupillometry data using a general linear convolution model [44,49,51,52], comparing the evidence for each model using Bayesian general linear regression [53]. The prior expectation of regression parameters were set to 0 within uninformative prior variance. The results presented below were robust to changes in this prior variance. This Bayesian general linear model (GLM) allows us to balance the increase in accuracy from additional regressors in models 1–6 with the accompanying increase in complexity. We convolved our stimuli with 5 gamma functions (with associated parameters), which can be reasonably expected to model the pupillary response to our stimuli —in the spirit of a pupillary response function; i.e., the pupillary response to neuronal afference (modelled by inferred precision). While 5 gamma functions are not required to model pupillary dilation (indeed, analysis of the parameters of each gamma function suggest only the widest gamma function is necessary), we did not want to make any prior assumptions about the pupillary response function, and therefore began with a range of possible functions. We retain this full range to allow for the simulations shown in the results section.

Table 1. Model designs.

Model 1 Photic Stimulation	**Model 2** Photic Stimulation Interaction Effects
Model 3 Photic Stimulation Inferred Precision	**Model 4** Photic Stimulation Interaction Effects Inferred Precision

https://doi.org/10.1371/journal.pcbi.1007126.t001

Photic stimulation was modelled as a boxcar function encoding the presence of a stimulus, the interaction term is the mean centred product of the simulated precision and the optical effects, while the precision terms are generated as described above. These explanatory variables are then convolved with a basis set comprising (five) gamma functions, such that the design matrix for model 3 has 10 columns. We added a constant term to account for the z-scoring performed in the pre-processing. Examples of these design matrices for a β–1 of 1.75 are shown in Fig 7. Model comparisons are performed with flat priors over each model, to avoid favouring one model over another.

Results

Treating model 1 as a null hypothesis, we test the alternate hypotheses to see if they provide a better explanation of the data. The results are shown in Fig 8, with the log model evidence relative to that of the null model (and the R^2 value to quantify the model fits to the grand mean data) provided for the other models. Model evidence can be read as the probability that a given model would generate the data at hand. The relative (log) model evidence between two models indicates how much better an explanation one model (or hypothesis) is for some given data set compared to another. Crucially, this considers both the accuracy and the complexity of the model, such that larger model evidence indicates that the model either accounts for the data with greater accuracy, or is a simpler explanation with comparable accuracy. This is closely related to other approaches for comparing models, including the Akaike information criterion (AIC) and the Bayesian information criterion (BIC).

Technically, model evidence is the log likelihood (accuracy) minus a (complexity) penalty for the effective number of model parameters. The AIC and BIC may be regarded as approximations to log model evidence, while statistics such as R^2 reflect accuracy. The key difference between accuracy and log evidence is that log evidence (and its free energy bound) penalises models whose parameters must be moved from their default (prior) values to explain the data (as measured by the Kullback0Lieber divergence between posterior and prior). The AIC and BIC approximate this complexity, but do not take account of whether or not these parameters are used to explain the data. In most model comparison settings, the variational free energy is a better approximation to (log) model evidence than the AIC or BIC [54].

In the current application of model comparison, we compare models for a range of prior beliefs from 0.3 to 20. Effectively, this is a line search for the optimal prior belief, relative to the null model (which has no dependence on the prior beliefs). Fig 8 shows that at very low prior beliefs, the more complicated model (model 4) is superior, but from a prior precision of $\beta^{-1} > 2.25$ the simpler model (model 3) is sufficient. Furthermore, the results confirm that pupillary responses are highly dependent on the β^{-1} (as suggested in Eq 2), and importantly that our model comparison can detect this dependency. With this in mind, we proceeded with a more delicate analysis, using model 3 (since it is superior to the other models over a larger range of precisions, and in particular around the most interesting range of precisions, see Fig 9) to examine the differences among our 9 participants.

Identification of participant prior beliefs

We may perform the same analysis used above (a Bayesian linear regression with uniform priors) to optimise the model of data generated by each of the 9 participants. This allows one to identify the optimal prior precision for each participant. To do this, following the regression analysis, we can pass the log model evidence of model 3 –for different prior precisions— through a softmax function [53,55] to obtain the posterior probability over prior precision.

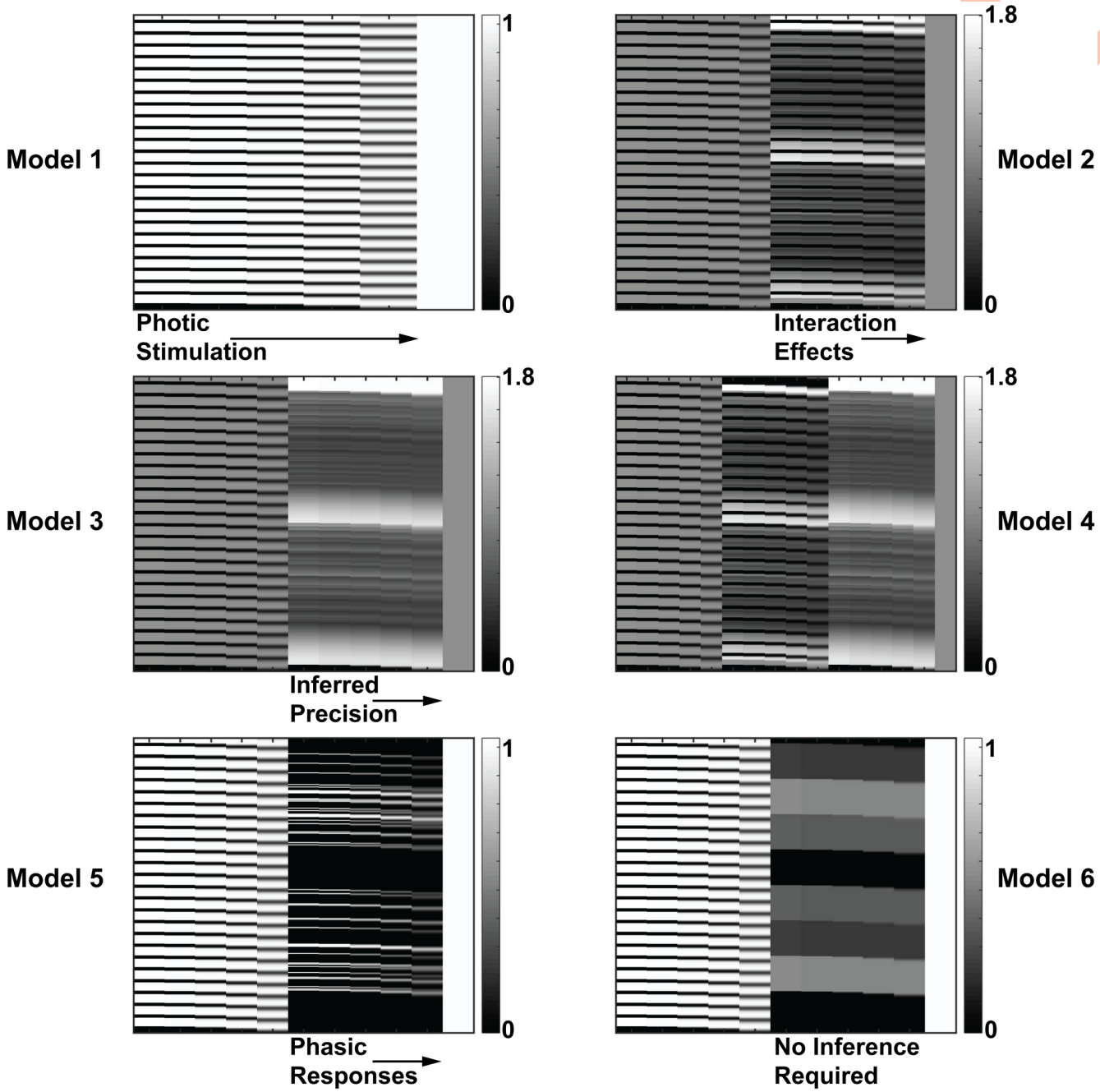

Fig 7. Example design matrices. Design matrices for models 1–6, corresponding to the stimuli detailed in Table 1 and the additional two naïve models (models 5 and 6). Each column indicates a single regressor, while each row is a point in time. In each model the final column (un-numbered) is a constant factor that accounts for the z-scoring performed in the pre-processing. The scale bar on the right indicates the values of the cells in the matrix.

https://doi.org/10.1371/journal.pcbi.1007126.g007

These results are shown in Fig 9, which shows the posterior probabilities for each of the 9 participants.

In Fig 9, we also report a confusion matrix, constructed by simulating data with different prior precisions (rows), and then computing the posterior probability afforded to each level of prior precision (columns) by each simulated dataset. This is to demonstrate that—if we

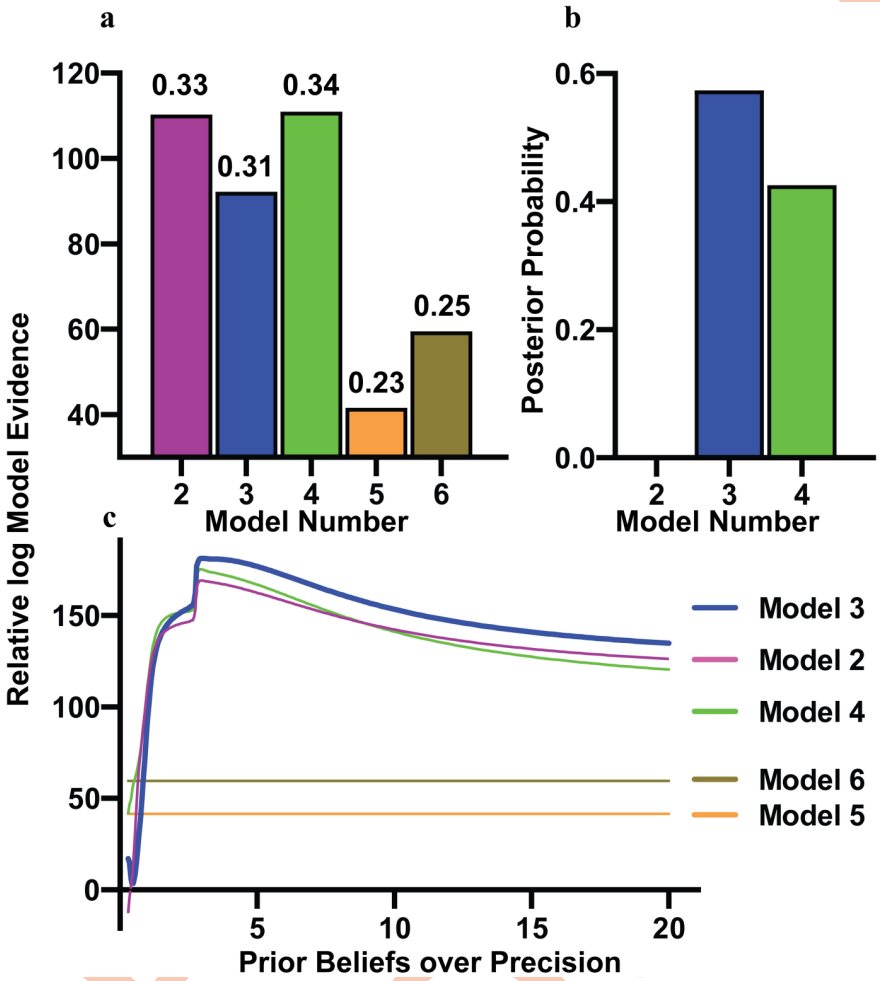

Fig 8. Bayesian comparison of alternative models relative to the null model. Fig 8a shows a bar plot of the log model evidence relative to that of the null model at a prior precision of 1, with the R^2 scores for each fit provided above each bar (the lowest of our candidates, see Fig 9a). Fig 8b shows the posterior probabilities of the models, calculated by passing the log model evidence through a softmax function. In the case of Fig 8b, we take the model comparison conducted at a prior precision of $\beta^{-1} = 2.25$, to justify the model selected in the next section. Fig 8c shows the log model evidence for models 2–6 relative to that of model 1 (the null model), plotted against the prior belief over precision used to generate the design matrix for each mode, and can be thought of as a series of individual model comparisons. The curve for model 3 is in bold to indicate this is the model used for the analysis of participant's prior beliefs. Note that the null model and models 5–6 do not depend on inferred precision and are therefore invariant to the prior beliefs. These results show that models explicitly containing inferred precision perform better over the range of prior beliefs considered, with the simpler model (model 3) performing best for $\beta^{-1} > 2.25$.

https://doi.org/10.1371/journal.pcbi.1007126.g008

simulate data—we can easily recover the parameter used to generate the simulations (demonstrating the sensitivity of our measure). To illustrate the face validity of this approach, we simulated data using the parameter values inferred for 4 of the participants. The correspondence between these and the measured data are shown Fig 9c–9f.

Fig 9a shows that our participants displayed a range of β^{-1}, with three below the average, four close to the average and two with slightly higher β^{-1}. Importantly, we are able to identify an optimal value for all participants. This conclusion is reinforced by Fig 9b, where we show that if we generate simulated time series for 5 similar values of β^{-1}, we can accurately assign the precisions to the correct simulation; through model comparison of models with different prior precisions.

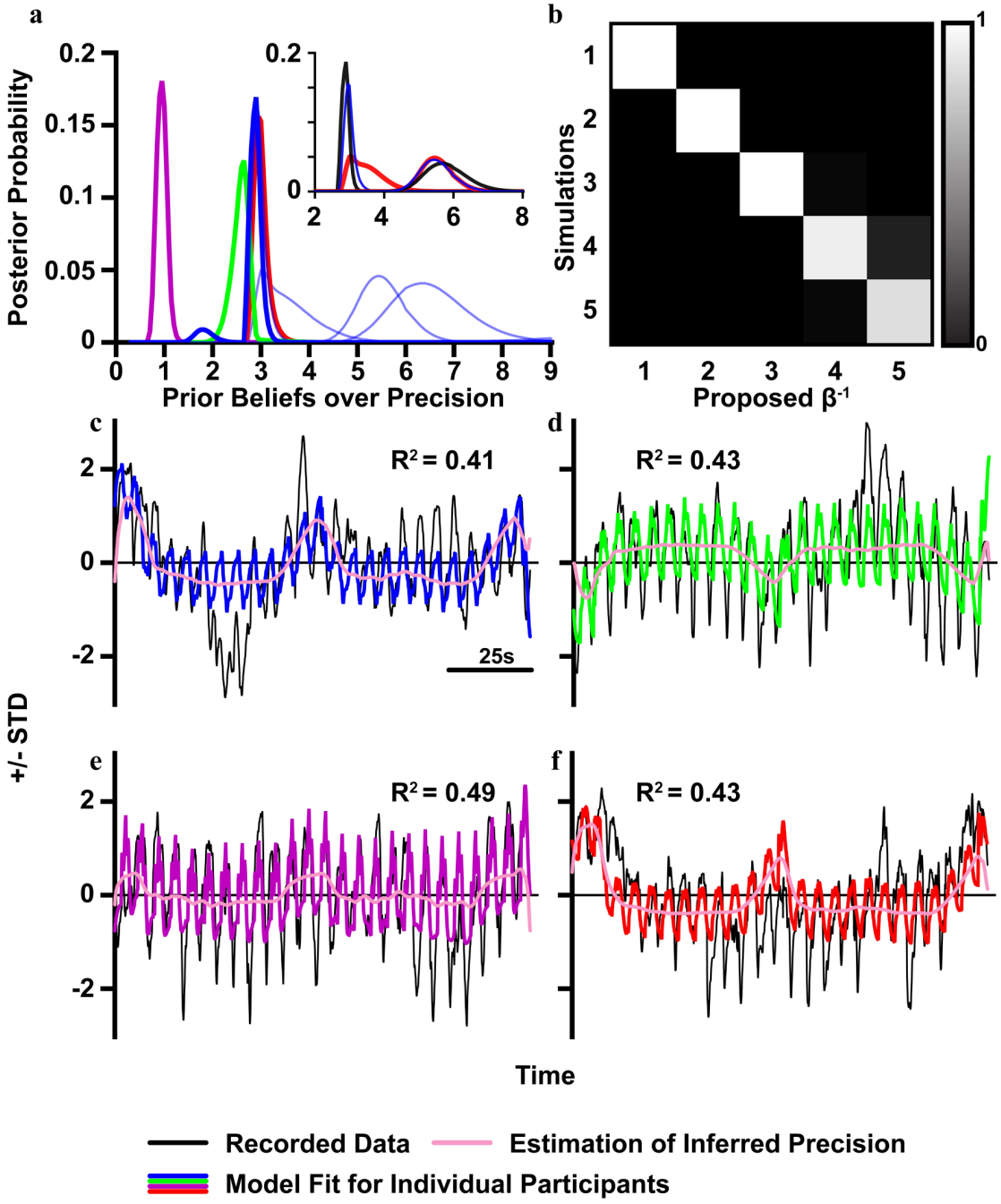

Fig 9. Estimating participants prior beliefs over precision. Using a Bayesian model comparison, we can calculate a posterior distribution over prior beliefs about precision using the evidence for models of observed data, under each level of prior precisions considered. In Fig 9a, posterior distributions for individual participants are shown in blue for 5 of 9, while the remaining 4 are given colours that correspond to their models in parts c-f. The insert for Fig 9a shows the results for two participants when we analyse the data for the different sequences separately, with the red curves indicating the estimated prior precision for the sequences with imprecise A and B matrices, and the black showing the estimated prior precision for sequences with only an imprecise B matrix. The blue lines replicate the data in the main part of Fig 9a, with the two sequences combined. In Fig 9b we show a 'confusion' matrix, where the elements show the probability that the prior precision represented by the column was the value used to generate the simulated data represented in each row. Figs 9c-f show the simulated data generated with the most likely prior precision, in the colours given in Fig 9a, overlaid on the recorded data (in black). The estimation of the participant's inferred precision is also provided in pink, to show the contribution of precision to the model fit, as well as to show the fine scale tracking and responsive of pupil diameter to changes in

environmental volatility. The four participants shown had the highest posterior probability in the estimation of their prior beliefs over precision. R^2 values are given for the model fits for the 4 participants shown.

https://doi.org/10.1371/journal.pcbi.1007126.g009

This characterisation of model identifiability is reflected in the fact that the highest probabilities lie on the (confusion) matrix diagonal. In other words, we can recover the correct model that generated pupillometry data based on, and only on, the data themselves. To characterise the simulations that are used to find the optimal prior precision, in Fig 9c–9f we overlay the simulations on the recorded data for 4 participants, showing that the regression parameters can be used to generate plausible data. Note in Fig 9c there is a large deviation between the simulation and the recorded data around 400ms; this might explain the double peak seen in the thick blue trace in Fig 9a.

Discussion

To establish the role of inferred precision (inverse volatility) in explaining pupillometry data, we considered 6 models, each of which has a unique physiological interpretation. Model 1 proposed that optical factors alone are sufficient to explain the data. Had Model 1 won over the others, this would have represented evidence against our hypothesis; namely, that pupil dilation tracks inferred volatility. However, we show that models 2–4—all of which include the inferred precision in some form—are superior to the optical model. Furthermore, the results suggest that the model with inferred precision acting directly on the pupil diameter (Model 3) is the most effective over the largest range of prior precisions; including for the prior precisions shared by most of the participants. Interactions between inferred precision and optical effects have little explanatory value for these data. This suggests that the effect of precision on pupil diameter is distinct and separable from the optical impact (within the bounds of maximum and minimum pupil diameter). Finally, we are able to estimate, in a Bayes optimal fashion, the prior precision for our participants, demonstrating the sensitivity of this estimation in relation to intersubject variability.

While the results presented here are highly complementary to those in previous work taking a Bayesian perspective on pupillary dynamics (most notably by Nassar et al, 2012 and Krishnamurthy et al 2017, 6,31), our approach offers two additional benefits. First, our focus is on inference, as opposed to learning. Intuitively, this generalises previous approaches that focus on the optimisation of parameters of a generative model (learning) to accommodate beliefs about current states of the world (inference), and their changeability. Second, we have formulated our generative model to be consistent with a Markov decision process formulation of Active Inference (16,18). The importance of this is threefold. This sort of model is equipped with a process theory that has been used to account for a range of behavioural and electrophysiological observations, affording it a face validity. In addition to this face validity, the capacity to use exactly the same model to generate pupillary responses and choice behaviour (or evoked EEG responses) provides an opportunity to test the predictive validity of our model. In future work, we hope to be able to use the estimated parameters from pupillary data for individual subjects (or groups of subjects) to predict what one might measure using (for example) electroencephalography. Finally, given established associations between other neurotransmitter systems and parameters of these generative models [2,22,56], we are now in a position to investigate the interactions between these systems (e.g. how does my uncertainty about the changeability of my environment influence my uncertainty in how I am going to act?).

While pupillary dilatation is typically associated with central noradrenergic signalling, it is notable that other neurotransmitter systems have also been correlated with these responses in both humans [57] and animals [58]. As such, the link between pupillary dilatation and the

precision of transitions demonstrated here could be a manifestation of other transmitter systems in addition to (or in place of) noradrenaline, as well as different sources of noradrenergic stimulation [59–62]. For these reasons, we can only conclude that neuronal processes upstream of fibres projecting to the pupillary muscles are engaged in estimation of precision (or volatility), and that noradrenaline is the likely substrate of this. However, to implicate noradrenaline with greater confidence, it will be necessary to dissociate this from alternative transmitters. This could be through fMRI, comparing activity in the locus coeruleus, dopaminergic midbrain, and basal forebrain nuclei. Alternatively, it could be through the use of pharmacological intervention, exploring whether a central noradrenergic blockade abolishes the responses observed here. These experiments, when paired with a suitable paradigm to probe changes in likelihood mappings, could be used to further explore the theories of Yu and Dayan and others [2,56,63,64] in probing the neurotransmitter systems that underlie different forms of uncertainty.

Given recent work on the role of aberrant prior beliefs in autism and anxiety disorders, we also suggest that the techniques introduced above could be used to quantify group differences between neurotypical persons and people with autism. In practical terms, this would provide clinicians with a tool to quantitatively phenotype patients and provide a diagnostic aid for autism. Recent findings suggest that these measures may correlate with the severity of symptoms [14]. This suggests there may be utility in this type of phenotyping in quantifying the effects of therapeutic interventions. However, if this was to be used as a diagnostic tool, a change in experimental paradigm would be needed; autism spectrum disorders are often diagnosed very early in life (around 3–4 years old) [65], an age at which children are often not yet able to count. The first step to such a tool would be to use the current paradigm to examine differences between a small group of neurotypical people and patients with autism, within the age range examined in this work (18–35). If these experiments were successful in finding differences between the two sets of participants, subsequent studies could examine the efficacy of the paradigm in younger age groups, adjusting the paradigm to suit those not yet able to count —and those who find it difficult to focus on the stimulus.

Finally, we refer to the introduction and our argument that belief updating over the precision of state transitions is essential for intelligent life. While this work simply shows that humans do appear to use Bayes optimal updating for beliefs regarding volatile state transitions, it provides a solid framework from which to launch further exploration of the subtleties of this precision updating, including its interaction with belief updating for precision of likelihood mappings and for actions. With a solid theoretical and practical understanding of these concepts, the leap to a general artificial intelligence would be less of a jump, and almost a trivial consequence of (variational) optimality principles.

Supporting information

S1 Data. Participant 1. Zip file containing the pupillometry data for participant 1.
(ZIP)

S2 Data. Participant 2. Zip file containing the pupillometry data for participant 2.
(ZIP)

S3 Data. Participant 3. Zip file containing the pupillometry data for participant 3.
(ZIP)

S4 Data. Participant 4. Zip file containing the pupillometry data for participant 4.
(ZIP)

S5 Data. Participant 5. Zip file containing the pupillometry data for participant 5.
(ZIP)

S6 Data. Participant 6. Zip file containing the pupillometry data for participant 6.
(ZIP)

S7 Data. Participant 7. Zip file containing the pupillometry data for participant 7.
(ZIP)

S8 Data. Participant 8. Zip file containing the pupillometry data for participant 8.
(ZIP)

S9 Data. Participant 9. Zip file containing the pupillometry data for participant 9.
(ZIP)

Acknowledgments

This experiment was performed using Cogent 2000 developed by the Cogent 2000 team at the FIL and the ICN and Cogent Graphics developed by John Romaya at the LON at the Wellcome Department of Imaging Neuroscience.

Author Contributions

Conceptualization: Peter Vincent, Thomas Parr, David Benrimoh, Karl J Friston.

Data curation: Peter Vincent, Thomas Parr.

Formal analysis: Peter Vincent, Thomas Parr.

Investigation: Peter Vincent.

Methodology: Peter Vincent, Thomas Parr, David Benrimoh, Karl J Friston.

Software: Peter Vincent, Thomas Parr.

Supervision: Karl J Friston.

Validation: Peter Vincent, Thomas Parr.

Visualization: Peter Vincent, Thomas Parr.

Writing – original draft: Peter Vincent, Thomas Parr, David Benrimoh, Karl J Friston.

Writing – review & editing: Peter Vincent, Thomas Parr, David Benrimoh, Karl J Friston.

References

1. Nieuwenhuis S, Aston-Jones G, Cohen JD. Decision making, the P3, and the locus coeruleus-norepinephrine system. Psychological Bulletin. 2005. pp. 510–532. https://doi.org/10.1037/0033-2909.131.4.510 PMID: 16060800
2. Yu AJ, Dayan P. Uncertainty, neuromodulation, and attention. Neuron. 2005; 46: 681–692. https://doi.org/10.1016/j.neuron.2005.04.026 PMID: 15944135
3. Lavín C, San Martín R, Rosales Jubal E. Pupil dilation signals uncertainty and surprise in a learning gambling task. Front Behav Neurosci. 2014; 7. https://doi.org/10.3389/fnbeh.2013.00218 PMID: 24427126
4. Liao HI, Yoneya M, Kidani S, Kashino M, Furukawa S. Human pupillary dilation response to deviant auditory stimuli: Effects of stimulus properties and voluntary attention. Front Neurosci. 2016; 10. https://doi.org/10.3389/fnins.2016.00043 PMID: 26924959
5. Preuschoff K, 't Hart BM, Einhäuser W. Pupil dilation signals surprise: Evidence for noradrenaline's role in decision making. Front Neurosci. 2011; 1–12.

6. Nassar MR, Rumsey KM, Wilson RC, Parikh K, Heasly B, Gold JI. Rational regulation of learning dynamics by pupil-linked arousal systems. Nat Neurosci. 2012; 15: 1040–1046. https://doi.org/10.1038/nn.3130 PMID: 22660479
7. Chapman RM, Bragdon HR. Evoked responses to numerical and non-numerical visual stimuli while problem solving. Nature. 1964; 203: 1155–1157. https://doi.org/10.1038/2031155a0 PMID: 14213667
8. Sutton S, Braren M, Zubin J, John ER. Evoked-Potential Correlates of Stimulus Uncertainty. Science (80-). 1965; 150: 1187–1188. https://doi.org/10.1126/science.150.3700.1187 PMID: 5852977
9. Feldman H, Friston KJ. Attention, Uncertainty, and Free-Energy. Front Hum Neurosci. 2010; 4. https://doi.org/10.3389/fnhum.2010.00215 PMID: 21160551
10. Donchin E, Coles MGH. Is the P300 component a manifestation of context updating? Behav Brain Sci. 1988; 11: 357–374. https://doi.org/10.1017/S0140525X00058027
11. Friston K. The free-energy principle: A unified brain theory? Nat Rev Neurosci. Nature Publishing Group; 2010; 11: 127–138. https://doi.org/10.1038/nrn2787 PMID: 20068583
12. Adams RA, Stephan KE, Brown HR, Frith CD, Friston KJ. The Computational Anatomy of Psychosis. Front Psychiatry. 2013; https://doi.org/10.3389/fpsyt.2013.00047 PMID: 23750138
13. Lawson RP, Rees G, Friston KJ. An aberrant precision account of autism. Front Hum Neurosci. 2014; 8. https://doi.org/10.3389/fnhum.2014.00302 PMID: 24860482
14. Lawson RP, Mathys C, Rees G. Adults with autism overestimate the volatility of the sensory environment. Nat Neurosci. 2017; 20: 4–6. https://doi.org/10.1038/nn.4615 PMID: 28758996
15. Friston K. Learning and inference in the brain. Neural Networks. 2003. pp. 1325–1352. https://doi.org/10.1016/j.neunet.2003.06.005 PMID: 14622888
16. Friston KJ, Parr T, de Vries B. The graphical brain: belief propagation and active inference. Netw Neurosci. 2017; 1–78.
17. Friston K, FitzGerald T, Rigoli F, Schwartenbeck P, O'Doherty J, Pezzulo G. Active inference and learning. Neurosci Biobehav Rev. Elsevier Ltd; 2016; 68: 862–879. https://doi.org/10.1016/j.neubiorev.2016.06.022 PMID: 27375276
18. Mirza MB, Adams RA, Mathys CD, Friston KJ. Scene Construction, Visual Foraging, and Active Inference. Front Comput Neurosci. 2016; 10. https://doi.org/10.3389/fncom.2016.00056 PMID: 27378899
19. Conant RC, Ross Ashby W. Every good regulator of a system must be a model of that system. Int J Syst Sci. 1970; 1: 89–97. https://doi.org/10.1080/00207727008920220
20. Friston K. The free-energy principle: a rough guide to the brain? Trends Cogn Sci. 2009; 13: 293–301. https://doi.org/10.1016/j.tics.2009.04.005 PMID: 19559644
21. Knill DC, Pouget A. The Bayesian brain: The role of uncertainty in neural coding and computation. Trends in Neurosciences. 2004. pp. 712–719. https://doi.org/10.1016/j.tins.2004.10.007 PMID: 15541511
22. Parr T, Friston KJ. Uncertainty, epistemics and active inference. J R Soc Interface. 2017; 14: 20170376. https://doi.org/10.1098/rsif.2017.0376 PMID: 29167370
23. Jepma M, Brown SBRE, Murphy PR, Koelewijn SC, De Vries B, van den Maagdenberg AM, et al. Noradrenergic and cholinergic modulation of belief updating. J Cogn Neurosci. 2018; https://doi.org/10.1162/jocn_a_01317 PMID: 30063180
24. Silvetti M, Seurinck R, van Bochove ME, Verguts T. The influence of the noradrenergic system on optimal control of neural plasticity. Front Behav Neurosci. 2013; https://doi.org/10.3389/fnbeh.2013.00160 PMID: 24312028
25. Gil Z, Connors BW, Amitai Y. Differential regulation of neocortical synapses by neuromodulators and activity. Neuron. 1997; https://doi.org/10.1016/S0896-6273(00)80380-3
26. Disney AA, Aoki C, Hawken MJ. Gain Modulation by Nicotine in Macaque V1. Neuron. 2007; https://doi.org/10.1016/j.neuron.2007.09.034 PMID: 18031686
27. Moran RJ, Campo P, Symmonds M, Stephan KE, Dolan RJ, Friston KJ. Free Energy, Precision and Learning: The Role of Cholinergic Neuromodulation. J Neurosci. 2013; https://doi.org/10.1523/JNEUROSCI.4255-12.2013 PMID: 23658161
28. Vossel S, Geng JJ, Fink GR. Dorsal and ventral attention systems: Distinct neural circuits but collaborative roles. Neuroscientist. 2014; https://doi.org/10.1177/1073858413494269 PMID: 23835449
29. Marshall L, Mathys C, Ruge D, de Berker AO, Dayan P, Stephan KE, et al. Pharmacological Fingerprints of Contextual Uncertainty. PLoS Biol. 2016; https://doi.org/10.1371/journal.pbio.1002575 PMID: 27846219
30. Sales AC, Friston KJ, Jones MW, Pickering AE, Moran RJ. Locus Coeruleus tracking of prediction errors optimises cognitive flexibility: an Active Inference model. bioRxiv. 2018; 340620. https://doi.org/10.1101/340620

31. Osman M. Controlling Uncertainty: A Review of Human Behavior in Complex Dynamic Environments. Psychol Bull. 2010; https://doi.org/10.1037/a0017815 PMID: 20063926

32. Tenenbaum JB, Griffiths TL, Kemp C. Theory-based Bayesian models of inductive learning and reasoning. Trends Cogn Sci. 2006; https://doi.org/10.1016/j.tics.2006.05.009 PMID: 16797219

33. Meyer R, Yu J. Bugs for a Bayesian Analysis of Stochastic Volatility Models. SSRN. 2001. https://doi.org/10.2139/ssrn.267491

34. So MEP, Lam K, Li WK. A stochastic volatility model with markov switching. J Bus Econ Stat. 1998; https://doi.org/10.1080/07350015.1998.10524758

35. Berry T, Giannakis D, Harlim J. Nonparametric forecasting of low-dimensional dynamical systems. Phys Rev E—Stat Nonlinear, Soft Matter Phys. 2015; https://doi.org/10.1103/PhysRevE.91.032915 PMID: 25871180

36. Mathys CD, Lomakina EI, Daunizeau J, Iglesias S, Brodersen KH, Friston KJ, et al. Uncertainty in perception and the Hierarchical Gaussian Filter. Front Hum Neurosci. 2014; https://doi.org/10.3389/fnhum.2014.00825 PMID: 25477800

37. Nassar MR, Wilson RC, Heasly B, Gold JI. An Approximately Bayesian Delta-Rule Model Explains the Dynamics of Belief Updating in a Changing Environment. J Neurosci. 2010; 30: 12366–12378. https://doi.org/10.1523/JNEUROSCI.0822-10.2010 PMID: 20844132

38. Behrens TEJ, Woolrich MW, Walton ME, Rushworth MFS. Learning the value of information in an uncertain world. Nat Neurosci. 2007; 10: 1214–1221. https://doi.org/10.1038/nn1954 PMID: 17676057

39. Sutton RS, Barto AG. Reinforcement learning: An introduction. Cambridge, MA: MIT Press; 1998.

40. Parr T, Rees G, Friston KJ. Computational Neuropsychology and Bayesian Inference. Front Hum Neurosci. 2018; https://doi.org/10.3389/fnhum.2018.00061 PMID: 29527157

41. Krishnamurthy K, Nassar MR, Sarode S, Gold JI. Arousal-related adjustments of perceptual biases optimize perception in dynamic environments. Nat Hum Behav. 2017; https://doi.org/10.1038/s41562-017-0107 PMID: 29034334

42. Schwartenbeck P, Friston K. Computational Phenotyping in Psychiatry: A Worked Example. eNeuro. 2016; 3: ENEURO.0049-16.2016. https://doi.org/10.1523/ENEURO.0049-16.2016 PMID: 27517087

43. Peavler WS. Pupil Size, Information Overload, and Performance Differences. Psychophysiology. 1974; 11: 559–566. https://doi.org/10.1111/j.1469-8986.1974.tb01114.x PMID: 4415394

44. Hoeks B, Levelt WJM. Pupillary dilation as a measure of attention: a quantitative system analysis. Behav Res Methods, Instruments, Comput. 1993; https://doi.org/10.3758/BF03204445

45. Zekveld AA, Koelewijn T, Kramer SE. The Pupil Dilation Response to Auditory Stimuli : Current State of Knowledge. Trends Hear. 2018; 22: 1–25. https://doi.org/10.1177/2331216518777174 PMID: 30249172

46. Quirins M, Marois C, Valente M, Seassau M. Conscious processing of auditory regularities induces a pupil dilation. Sci Rep. 2018; 1–11.

47. Parr T, Friston KJ. The active construction of the visual world. Neuropsychologia. Elsevier Ltd; 2017; 104: 92–101. https://doi.org/10.1016/j.neuropsychologia.2017.08.003 PMID: 28782543

48. Lemercier A, Guillot G, Courcoux P, Garrel C, Baccino T, Schlich P. Pupillometry of taste: Methodological guide—from acquisition to data processing—and toolbox for MATLAB. Quant Methods Psychol. 2014; 10: 179–199.

49. Knapen T, De Gee JW, Brascamp J, Nuiten S, Hoppenbrouwers S, Theeuwes J. Cognitive and ocular factors jointly determine pupil responses under equiluminance. PLoS One. 2016; 11: 1–13. https://doi.org/10.1371/journal.pone.0155574 PMID: 27191166

50. Kiebel SJ, Friston KJ. Statistical parametric mapping for event-related potentials: I. Generic considerations. Neuroimage. 2004; https://doi.org/10.1016/j.neuroimage.2004.02.012 PMID: 15193578

51. Friston KJ, Jezzard P, Turner R. Analysis of functional MRI time-series. Hum Brain Mapp. 1994; 1: 153–171. https://doi.org/10.1002/hbm.460010207

52. de Gee JW, Knapen T, Donner TH. Decision-related pupil dilation reflects upcoming choice and individual bias. Proc Natl Acad Sci. 2014; https://doi.org/10.1073/pnas.1317557111 PMID: 24449874

53. Penny WD, Kilner J, Blankenburg F. Robust Bayesian general linear models. Neuroimage. 2007; 36: 661–671. https://doi.org/10.1016/j.neuroimage.2007.01.058 PMID: 17482836

54. Penny WD. Comparing Dynamic Causal Models using AIC, BIC and Free Energy. Neuroimage. 2012; 59: 319–330. https://doi.org/10.1016/j.neuroimage.2011.07.039 PMID: 21864690

55. Bishop CM. Pattern Recognition and Machine Learning [Internet]. Pattern Recognition. 2006. https://doi.org/10.1117/1.2819119

56. Schwartenbeck P, FitzGerald THB, Mathys C, Dolan R, Friston K. The dopaminergic midbrain encodes the expected certainty about desired outcomes. Cereb Cortex. 2015; https://doi.org/10.1093/cercor/bhu159 PMID: 25056572

57. de Gee JW, Colizoli O, Kloosterman NA, Knapen T, Nieuwenhuis S, Donner TH. Dynamic modulation of decision biases by brainstem arousal systems. Elife. 2017; https://doi.org/10.7554/eLife.23232 PMID: 28383284

58. Reimer J, McGinley MJ, Liu Y, Rodenkirch C, Wang Q, McCormick DA, et al. Pupil fluctuations track rapid changes in adrenergic and cholinergic activity in cortex. Nat Commun. 2016; https://doi.org/10.1038/ncomms13289 PMID: 27824036

59. Levitt P, Moore RY. Noradrenaline neuron innervation of the neocortex in the rat. Brain Res. 1978; https://doi.org/10.1016/0006-8993(78)90925-3

60. Levitt P, Moore RY. Origin and organization of brainstem catecholamine innervation in the rat. J Comp Neurol. 1979; https://doi.org/10.1002/cne.901860402 PMID: 15116686

61. Loewenfeld IE, Lowenstein O. The pupil: anatomy, physiology, and clinical applications. Ames: Iowa State University Press; 1993.

62. Nieuwenhuis S, De Geus EJ, Aston-Jones G. The anatomical and functional relationship between the P3 and autonomic components of the orienting response. Psychophysiology. 2011. https://doi.org/10.1111/j.1469-8986.2010.01057.x PMID: 20557480

63. Howard CD, Li H, Geddes CE, Jin X. Dynamic Nigrostriatal Dopamine Biases Action Selection. Neuron. 2017; https://doi.org/10.1016/j.neuron.2017.02.029 PMID: 28285820

64. Jepma M, Murphy PR, Nassar MR, Rangel-Gomez M, Meeter M, Nieuwenhuis S. Catecholaminergic Regulation of Learning Rate in a Dynamic Environment. PLoS Comput Biol. 2016; https://doi.org/10.1371/journal.pcbi.1005171 PMID: 27792728

65. American Psychiatric Association. DSM-V. American Journal of Psychiatry. 2013.